33rd Symposium on Naval Hydrodynamics
Osaka, Japan, 18-23 October 2020

Numerical analysis of semi-displacement vessels in head waves

H. Simonis[1], P. Marleaux[1], and M. Abdel-Maksoud[1]
([1]Institute for Fluid Dynamics and Ship Theory, Hamburg University of Technology (TUHH), Hamburg, Germany)

ABSTRACT

A numerical method for the computation of the dynamic behaviour of high-speed ships in waves is presented. The method is based on 2D+t theory, in which the three-dimensional (3D) flow around the vessel is replaced by several two-dimensional (2D) flows in earth-fixed transverse cross planes. The time development of the two-dimensional flows caused by the ship advancing through these transverse cross planes is computed. Together the two-dimensional flows give an approximation of the original three-dimensional flow. This approach simplifies the computations significantly and is appropriate for fast and slender ships since the flow will change only slowly along the ship. However, three-dimensional effects may still matter in some cases. The two-dimensional flows are treated as fully nonlinear potential flows. This means that viscous effects are neglected and that boundary conditions are kept in their nonlinear form and fulfilled on the instantaneous wetted hull and free surface. Therefore, most of the nonlinear effects can be taken into account. A boundary element method (BEM) is then used to calculate the flow numerically. A separation model is employed so that the non-viscous flow separation from round bilges can be computed. The developed method is used to compute the motions and forces on a semi-displacement vessel at high forward speed in calm water and also in incoming waves, which has not been achieved before using such a method. The results are compared to experimental data and generally very satisfactory agreement is found.

INTRODUCTION

There is a large number of high-speed vessels operating at Froude numbers roughly between 0.5 and 1.0, e.g. patrol or rescue vessels. At these speeds both gravity related and hydrodynamic pressure forces caused by the flow around the hull are of similar importance. Therefore, ships operating in this speed range can be called semi-displacement vessels (Faltinsen, 2005).

In most cases the hulls of semi-displacement vessels have high beam-to-draft ratios and round bilges. While the hulls are usually quite slender in the forward sections they are often wide at the transom stern. While a wide dry transom stern causes damping in waves and thus improves the seakeeping behaviour it may not be beneficial with respect to the resistance in calm water (Blok and Beukelman, 1984). However, that is not necessarily the case in the whole speed range as the transom stern also influences the creation of dynamic lift and therefore affects the rise and trim of the ship (Lugni et al., 2004). Therefore, a hydrodynamic evaluation both in calm water and in waves is very important to ensure good performance in all operating conditions.

Such an evaluation may be difficult due to certain features of the flow around a semi-displacement vessel. In calm water the steady flow due to a high forward speed often exhibits a highly deformed free surface. Steep breaking waves may be present and flow separation can occur at the stern but also from the round bilges as the ship speed increases. In waves, the wetted hull shape may change significantly which has an influence on the hydrodynamic forces acting on the ship.

If a hydrodynamic evaluation is to be carried out numerically, there are many different methods available, of which all have certain advantages and disadvantages. A well-established method to compute the motions of a ship in waves is the linear strip method (Salvesen et al. 1970). This method is highly efficient but simplifies the problem of a ship travelling in waves to a large extent. It linearizes the governing equations and neglects three-dimensional and viscous flow effects, as well as the interaction between steady flow due to the forward motion and unsteady flow due to ship motions and incident waves. Especially the last assumption is questioned widely for high-speed ships (Faltinsen, 2005; Sun and Faltinsen, 2011). However, it has been shown that also in that case useful results can be obtained (Blok and Beukelman, 1984). More advanced methods include 3D Boundary Element Methods (BEM). Lugni et al. (2004) used two different kinds of linear 3D BEM to study the behaviour of slender semi-displacement monohulls and

catamarans in calm water and regular head waves up to Froude number 0.8. One method linearizes the flow about the undisturbed inflow (Neumann-Kelvin linearization, NK) and the other method linearizes the flow about the double body flow (double body linearization, DM). The Neumann-Kelvin linearization essentially neglects the interaction between the steady flow and the unsteady flow. The double body linearization accounts for it partly, but is more valid at lower Froude numbers. Both methods produced reasonable results, although the BEM using double body linearization performed better, especially when looking at the computed pitch amplitudes. Ommani (2013) also developed a 3D BEM using Neumann-Kelvin linearization and applied it to study semi-displacement vessels. He improved the method in such a way that the dry transom stern could be accounted for, leading to improved results. A fully nonlinear 3D BEM does not use any linearization of the governing equations and is therefore more accurate by accounting for all nonlinearities, but also more demanding with respect to computational resources. Mola et al. (2017) used a fully nonlinear BEM to compute the flow around the DTMB-5415 hull and the NPL hull at steady forward speed in calm water up to Froude numbers of 0.4. They also accounted for the dry transom stern. However, they modified the free surface boundary condition at the highest Froude numbers to suppress wave breaking and improve the stability of the computations. They believed this to be the main reason for observed deviations of computed resistance values from the experimental results. Reynolds-Averaged Navier-Stokes (RANS) methods account for viscous effects and are routinely used nowadays when studying the hydrodynamic behaviour of high-speed ships and very accurate results can be obtained (Zlatev, 2009). However, the computational effort is also quite high.

Much less computing power is needed if methods based on 2D+t theory are employed. In a method based on 2D+t theory the three-dimensional flow problem around the ship is replaced by several two-dimensional flow problems in earth-fixed transverse cross planes, see Fig. 1. The time development of the two-dimensional flows caused by the movement of the ship through these cross planes is computed. Together the two-dimensional flow problems approximate the original three-dimensional flow problem. The two-dimensional flow problems in the cross planes are solved separately and are not directly coupled with each other. The assumption behind this simplification is, that the flow changes much more in the transverse direction than in the longitudinal direction. As a result, many three-dimensional effects, e.g. the transverse wave system induced by the ship, are neglected. This assumption is justified if the ship is sufficiently slender (i.e. dimensions in the longitudinal direction are much larger than in the transverse direction) and the Froude number is high, so that the influence of the transverse waves of the ship is negligible. However, as pointed out by Ommani (2013), near the transom stern three-dimensional effects may matter. At a dry transom the pressure has to be atmospheric and consequently the sectional forces vanish here. This cannot be accounted for by the 2D+t method since the pressure drop towards the transom stern is a consequence of the variation of the flow in the longitudinal direction in front of the transom stern. Sun and Faltinsen (2011) used a 2D+t method to study the behaviour of prismatic planing vessels in head waves and forced heave motions of a semi-displacement vessel in calm water (Sun and Faltinsen, 2012). The method used here is based on that approach and extends it to consider free motions of semi-displacement vessels in incoming waves.

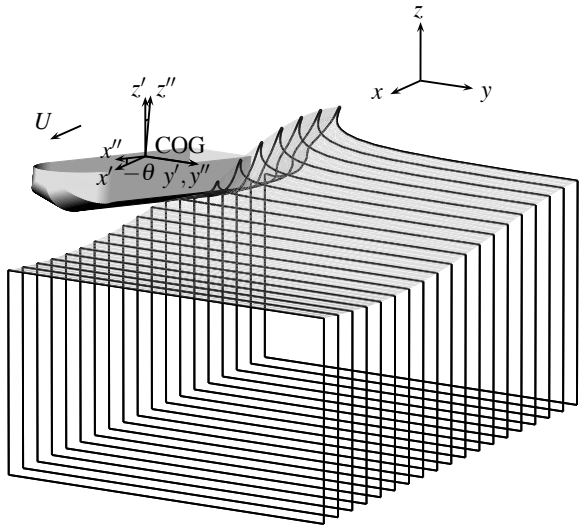

Figure 1: In a 2D+t method, the three-dimensional flow is approximated by several two-dimensional flow problems in earth-fixed transverse cross planes. Because of the symmetry of the cases investigated here, only one half of the fluid domain is considered.

In this paper a 2D+t method is used to study the free motions of a semi-displacement vessel in head waves. In the following part of the paper the method is outlined briefly. Then the method is used to compute the forces acting on a semi-displacement vessel at steady forward motion in calm water. After that the results obtained for forced heave motions in calm water and free heave and pitch motions in regular head waves are presented. The results are compared to experiments carried out by Keuning (1988) and Blok and Beukelman (1984).

METHOD DESCRIPTION

Governing equations

For the computations an earth-fixed coordinate system xyz is introduced, see Figure 1. The z-axis points

vertically upward and the x- and the y-axes coincide with the undisturbed free surface. Furthermore, a coordinate system $x'y'z'$ is used, which has its origin at the center of gravity (COG) of the ship but is not rotated with respect to the coordinate system xyz. Also, a coordinate system $x''y''z''$ is used, which is fixed to the ship and has its origin at the COG. The earth-fixed coordinates of the ship's center of gravity are denoted by x_G, y_G, z_G, while $y_G \equiv 0$. Since only heave and pitch motions of a ship moving ahead at a constant forward speed U are considered, it follows that

$$\begin{bmatrix} x - x_G \\ y - y_G \\ z - z_G \end{bmatrix} = \begin{bmatrix} x' \\ y' \\ z' \end{bmatrix} = \begin{bmatrix} \cos\theta & 0 & \sin\theta \\ 0 & 1 & 0 \\ -\sin\theta & 0 & \cos\theta \end{bmatrix} \begin{bmatrix} x'' \\ y'' \\ z'' \end{bmatrix}, \quad (1)$$

θ being the trim angle of the ship. The velocity of a point $\mathbf{x}_B = x_B\mathbf{i} + y_B\mathbf{j} + z_B\mathbf{k}$ on the surface of the ship's hull is then given by

$$\mathbf{v}_B = \left(U + \dot{\theta}(z_B - z_G)\right)\mathbf{i} + \left(\dot{z}_G - \dot{\theta}(x_B - x_G)\right)\mathbf{k}, \quad (2)$$

where $\mathbf{i}$, $\mathbf{j}$ and $\mathbf{k}$ are the unit vectors in the x-, y- and z-directions, respectively.

The flow is considered as potential flow, which is determined by the total velocity potential $\Phi = \Phi(x, y, z, t)$. This fulfils the three-dimensional Laplace equation

$$\frac{\partial^2\Phi}{\partial x^2} + \frac{\partial^2\Phi}{\partial y^2} + \frac{\partial^2\Phi}{\partial z^2} = 0 \quad (3)$$

with the boundary conditions

$$\frac{\mathrm{D}\Phi}{\mathrm{D}t} = \frac{1}{2}\left(\frac{\partial\Phi}{\partial x}\right)^2 + \frac{1}{2}\left(\frac{\partial\Phi}{\partial y}\right)^2 + \frac{1}{2}\left(\frac{\partial\Phi}{\partial z}\right)^2 - gz, \quad (4)$$

$$\frac{\mathrm{D}x}{\mathrm{D}t} = \frac{\partial\Phi}{\partial x}, \frac{\mathrm{D}y}{\mathrm{D}t} = \frac{\partial\Phi}{\partial y}, \frac{\mathrm{D}z}{\mathrm{D}t} = \frac{\partial\Phi}{\partial z} \quad (5)$$

at the free surface and

$$\nabla\Phi \cdot \mathbf{n} = \mathbf{v}_B \cdot \mathbf{n} \quad (6)$$

on the hull. In the above equations $\mathbf{n}$ denotes the normal vector pointing out of the fluid domain, which has the coordinates n_x, n_y, n_z in the earth-fixed coordinate system and g is the acceleration of gravity. Eq. (4) follows from Bernoulli's equation using

$$\frac{\mathrm{D}}{\mathrm{D}t} = \frac{\partial}{\partial t} + \nabla\Phi \cdot \nabla. \quad (7)$$

In order to account for long-crested head waves propagating in the negative x-direction, Φ is decomposed into an unknown disturbance potential ϕ, which needs to be computed, and a known wave potential $\phi_W = \phi_W(x, z, t)$, so that

$$\Phi = \phi + \phi_W. \quad (8)$$

To study ships in regular seaway, ϕ_W is prescribed using linear wave theory, i.e.

$$\phi_W = \frac{\omega\zeta_{WA}}{k} e^{kz} \cos(kx + \omega t). \quad (9)$$

Eq. (9) describes the velocity potential of a linear deep water wave propagating in the negative x-direction where ζ_{WA} is the wave amplitude, k is the wave number and ω is the wave frequency.

Both Φ and ϕ fulfil the three-dimensional Laplace equation with three-dimensional boundary conditions. However, the computation of ϕ can be simplified to a large extent if the flow is assumed to change much more in the transverse direction than in the longitudinal direction of the ship. This assumption is justified if the ship is slender, the ship's speed is high and the occurring trim angles as well as the steepness of the incoming waves remain small. If the slenderness parameter $\epsilon = B/L$ is introduced, where B is the ship's breadth and L is the ship's length, assuming a slender ship implies $\epsilon \ll 1$. In this case it can be deduced that $\partial/\partial x = O(\epsilon)$, $\partial/\partial y = O(1)$, $\partial/\partial z = O(1)$ and that $n_x = O(\epsilon)$, $n_y = O(1)$, $n_z = O(1)$. Furthermore, the Froude number $\mathrm{Fn} = U/\sqrt{gL} = O(1)$ as well as $\theta = O(\epsilon)$ and $\lambda/L = O(1)$ where λ is the length of the incoming waves. Sun and Faltinsen (2011) show that under these assumptions Eqs. (3) to (6) can be simplified if terms of the order of ϵ^2 are neglected. Using Eq. (8), ϕ is then determined by the two-dimensional Laplace equation

$$\frac{\partial^2\phi}{\partial y^2} + \frac{\partial^2\phi}{\partial z^2} = 0 \quad (10)$$

with the boundary conditions

$$\frac{\mathrm{D}\phi}{\mathrm{D}t} = -\frac{\partial\phi_W}{\partial t} + \frac{1}{2}\left(\frac{\partial\phi}{\partial y}\right)^2 + \frac{1}{2}\left(\frac{\partial\phi}{\partial z}\right)^2 - gz, \quad (11)$$

$$\frac{\mathrm{D}y}{\mathrm{D}t} = \frac{\partial\phi}{\partial y}, \frac{\mathrm{D}z}{\mathrm{D}t} = \frac{\partial\phi}{\partial z} + \frac{\partial\phi_W}{\partial z} \quad (12)$$

at the free surface and

$$\frac{\partial\phi}{\partial n} = \mathbf{v}_B \cdot \mathbf{n} - \nabla\phi_W \cdot \mathbf{n} \quad (13)$$

on the hull. The boundary value problem is completed by imposing

$$\frac{\partial\phi}{\partial n} = 0 \quad (14)$$

on the symmetry plane and on the outer boundaries, which are assumed sufficiently far away from the ship so that they do not influence the flow significantly. Here $\partial\phi/\partial n$ denotes the derivative of ϕ in the direction of the two-dimensional normal vector $n_y\mathbf{j} + n_z\mathbf{k}$. Eq. (10) states that ϕ is approximately determined by the two-dimensional Laplace equation in the yz-plane. Therefore, the three-dimensional flow can be replaced

by several two-dimensional flows in earth-fixed transverse cross planes, one of which is shown in Figure 2.

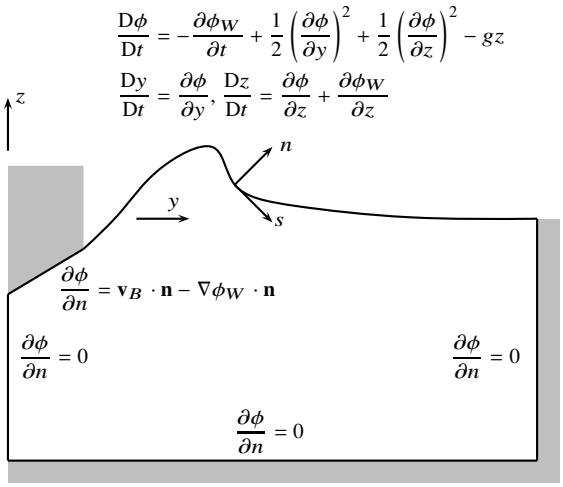

Figure 2: The flow in the transverse cross planes is considered as potential flow determined by a Dirichlet boundary condition on the free surface and a Neumann boundary condition on the hull and the outer boundaries.

Eqs. (10) to (14) may be used to compute the time development of the two-dimensional flows. The pressure on the hull may then be computed from Bernoulli's equation which can be written in the form of

$$p - p_0 = -\rho\left(\frac{\partial\phi}{\partial t} + \frac{\partial\phi_W}{\partial t} + \frac{1}{2}\left(\frac{\partial\phi}{\partial y}\right)^2 + \frac{1}{2}\left(\frac{\partial\phi}{\partial z}\right)^2 + \frac{\partial\phi}{\partial z}\frac{\partial\phi_W}{\partial z} + gz\right) \tag{15}$$

by using Eq. (8) and again neglecting terms of the order of ϵ^2. The local time derivative of the velocity potential $\partial\phi/\partial t$ is computed from

$$\frac{\partial\phi}{\partial t} = \frac{\mathrm{d}\phi}{\mathrm{d}t} - \dot{\mathbf{x}}_P \cdot \nabla\phi. \tag{16}$$

where $\mathrm{d}\phi/\mathrm{d}t$ denotes the time change of ϕ observed at the moving point $\mathbf{x}_P$ on the hull surface in the cross plane and $\dot{\mathbf{x}}_P$ is its velocity. Afterwards, forces and moments acting on the ship can be determined.

The motions of the ship can be computed from the equations of motion

$$\mathbf{M}\ddot{\boldsymbol{\xi}} = \mathbf{F} - \mathbf{F}_0 \tag{17}$$

where

$$\mathbf{M} = \begin{bmatrix} M & 0 \\ 0 & I_{55} \end{bmatrix} \qquad \boldsymbol{\xi} = \begin{bmatrix} \xi_3 \\ \xi_5 \end{bmatrix} \qquad \mathbf{F} = \begin{bmatrix} F_3 \\ F_5 \end{bmatrix}$$

and M is ship's mass, I_{55} is the mass moment of inertia with respect to the y-axis, F_3 is the lift force and F_5 is the pitch moment. Furthermore, $\xi_3 = z_G$ and $\xi_5 = \theta$ denote the heave and pitch motion, respectively. $\mathbf{F}_0$ contains the lift force and pitch moment acting on the ship in the equilibrium running condition. By accounting for $\mathbf{F}_0$ the right-hand side of Eq. (17) vanishes in the prescribed equilibrium running condition in calm water. In doing so, errors in the computation of the hydrodynamic forces are accounted for, which mainly occur due to the neglected influence of three-dimensional effects. The overestimated forces at the transom stern are generally the main source of error in this respect. Following Söding (2001) Eq. (17) is rewritten as

$$\frac{\mathrm{d}\boldsymbol{\xi}}{\mathrm{d}t} = \dot{\boldsymbol{\xi}} \tag{18}$$

$$\frac{\mathrm{d}\dot{\boldsymbol{\xi}}}{\mathrm{d}t} = \ddot{\boldsymbol{\xi}} = (\mathbf{M} + \mathbf{A})^{-1}(\mathbf{F} - \mathbf{F}_0 + \mathbf{A}\ddot{\boldsymbol{\xi}}) \tag{19}$$

in view of a stable numeric solution, where $\mathbf{A}$ is the added mass matrix. Here, the second-order differential equation (17) has also been rewritten as a system of two first-order differential equations.

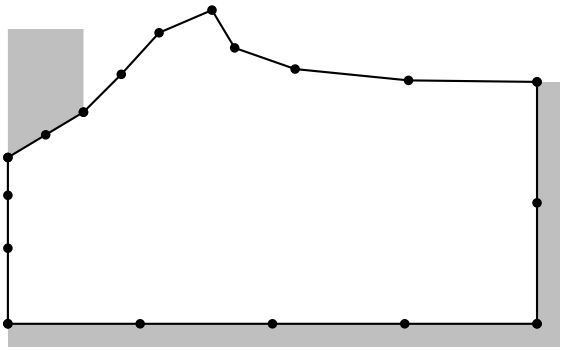

Figure 3: The boundary of the fluid domain is discretized using linear isoparametric elements. While the elements have the same size Δs on the hull and on the free surface near the hull, the size is increasing in the outer parts of the domain.

Numerical solution

In order to compute the time development of the flow within the cross planes, the boundary conditions on the free surface (11) and (12) are integrated. Eq. (11) may be used to obtain the time development of ϕ at the free surface and Eq. (12) can be used to obtain the change of the shape of the free surface. In order to evaluate the right hand sides of Eqs. (11) and (12), the boundary value problem for ϕ has to be solved so that $\partial\phi/\partial y$ and $\partial\phi/\partial z$ can be calculated. This is accomplished numerically using a BEM. Therefore, only the boundary of the cross plane has to be discretized. In this work this is done using linear isoparametric elements, i.e. both the variation of ϕ and

$\partial\phi/\partial n$ and the variation of the shape of the boundary are assumed to be linear over each element, see Fig. 3. To obtain a solution using the BEM, either ϕ or $\partial\phi/\partial n$ has to be specified at each node. On the free surface, the current values of ϕ are used and on the hull and the outer boundaries $\partial\phi/\partial n$ is prescribed using Eqs. (13) and (14). The solution then yields ϕ and $\partial\phi/\partial n$ at each node on the boundary of the cross plane. The velocities $\partial\phi/\partial y$ and $\partial\phi/\partial z$, which are needed to evaluate the right hand sides of Eqs. (11) and (12), can then be computed at each node from

$$\frac{\partial\phi}{\partial y} = \frac{\partial\phi}{\partial s}\frac{\partial y}{\partial s} - \frac{\partial\phi}{\partial n}\frac{\partial z}{\partial s}, \tag{20}$$

$$\frac{\partial\phi}{\partial z} = \frac{\partial\phi}{\partial s}\frac{\partial z}{\partial s} + \frac{\partial\phi}{\partial n}\frac{\partial y}{\partial s}, \tag{21}$$

where the normal velocity $\partial\phi/\partial n$ at the free surface is known from the solution of the boundary value problem. As before, n denotes the normal direction and s the tangential direction, see Fig. 2. The tangential derivatives $\partial\phi/\partial s$, $\partial y/\partial s$ and $\partial z/\partial s$ are calculated from the known values of ϕ, y and z at the free surface, respectively, by locally fitting a second order polynomial using the Moving Least Squares method as described by Wang (2005). The difference here is that the fit is carried out in one dimension with respect to the polygonal arc length. When the velocities at the free surface are known, Eqs. (11) and (12) can be evaluated and integrated for each node on the free surface. The solution of the flow is closely coupled to the solution of the equations of motions, which should be solved iteratively, as the acceleration also appears on the right hand side of Eq. (19). Therefore, a scheme based on the mixed implicit/explicit Euler scheme (Nakos et al., 1993) is devised here. The discretized forms of the equations used here are then

$$\frac{y^{n+1} - y^n}{\Delta t} = \left(\frac{\partial\phi}{\partial y}\right)^n \tag{22}$$

$$\frac{z^{n+1} - z^n}{\Delta t} = \left(\frac{\partial\phi}{\partial z} + \frac{\partial\phi_W}{\partial z}\right)^n \tag{23}$$

$$\frac{\phi^{n+1} - \phi^n}{\Delta t} = \left(-\frac{\partial\phi_W}{\partial t} + \frac{1}{2}\nabla\phi^2 - gz\right)^{n+1} \tag{24}$$

$$\frac{\partial\phi}{\partial n}^{n+1} = \mathbf{v}_B^{n+1}\cdot\mathbf{n}^{n+1} - \nabla\phi_W^{n+1}\cdot\mathbf{n}^{n+1} \tag{25}$$

$$\frac{\boldsymbol{\xi}^{n+1} - \boldsymbol{\xi}^n}{\Delta t} = \dot{\boldsymbol{\xi}}^n \tag{26}$$

$$\frac{\dot{\boldsymbol{\xi}}^{n+1} - \dot{\boldsymbol{\xi}}^n}{\Delta t} = (\mathbf{M}+\mathbf{A})^{-1}\left(\mathbf{F}^{n+1} - \mathbf{F}_0 + \mathbf{A}\ddot{\boldsymbol{\xi}}^{n+1}\right) \tag{27}$$

where $\partial\phi/\partial t$, which is needed for the computation of pressures and hence forces, is computed from

$$\frac{\partial\phi}{\partial t}^{n+1} = \frac{\phi^{n+1} - \phi^n}{\Delta t} - \frac{\mathbf{x}_P^{n+1} - \mathbf{x}_P^n}{\Delta t}\cdot\nabla\phi^{n+1}. \tag{28}$$

In the above equations upper indices n indicate the time step and should not be confused with the normal direction. Therefore, after evaluating the velocities at each node of the free surface, the position of each node at the free surface and on the hull is updated in an explicit Euler step according to Eqs. (22), (23) and (26). Then the velocity potential ϕ at the free surface and the body velocity $\dot{\boldsymbol{\xi}}$ are updated iteratively in an implicit Euler step according to Eqs. (24) and (27) until convergence is achieved. While iterating, $\partial\phi/\partial n$ and $\partial\phi/\partial t$ on the hull surface are always evaluated at the new time level, see Eqs. (25) and (28). Since the shape of the boundary is determined explicitly, the coefficient matrix necessary in the solution process using the BEM does not have to be recomputed during the iteration. That reduces the computational effort significantly. As described in more detail by Söding (2001), adding the term $\mathbf{A}\ddot{\boldsymbol{\xi}}$ on both sides of Eq. (17), which leads to Eq. (19), is only necessary to aid convergence and does not change that equation. No high accuracy is needed when determining $\mathbf{A}$. Therefore $\mathbf{A}$ is only updated, say, every 20 time steps so that it has the right order of magnitude but the computation times do not increase significantly. The computation of $\mathbf{A}$ is carried out by solving additional boundary value problems as described by Wu and Eatock-Taylor (1996) and Sichermann (2008). Having obtained the pressure distribution the sectional forces can be computed. The total forces are then obtained using a linear interpolation of the sectional forces. The sectional force at the front perpendicular is assumed to be zero while the force at the transom stern is calculated from an extrapolation of the sectional forces at the two cross planes in front of the transom stern.

During numerical tests it turned out that a first-order scheme was sometimes not accurate enough when updating the free surface. Therefore, a variant based on the second-order implicit/explicit trapezoidal rule was also implemented. In that scheme Eq. (22) is changed to

$$\begin{aligned}\frac{y^{n+1^\star} - y^n}{\Delta t} &= \left(\frac{\partial\phi}{\partial y}\right)^n \\ \frac{y^{n+1} - y^n}{\Delta t} &= \frac{1}{2}\left(\frac{\partial\phi}{\partial y}\right)^n + \frac{1}{2}\left(\frac{\partial\phi}{\partial y}\right)^{n+1^\star}\end{aligned} \tag{29}$$

while Eq. (23) is correspondingly changed to

$$\begin{aligned}\frac{z^{n+1^\star} - z^n}{\Delta t} &= \left(\frac{\partial\phi}{\partial z} + \frac{\partial\phi_W}{\partial z}\right)^n \\ \frac{z^{n+1} - z^n}{\Delta t} &= \frac{1}{2}\left(\frac{\partial\phi}{\partial z} + \frac{\partial\phi_W}{\partial z}\right)^n \\ &\quad + \frac{1}{2}\left(\frac{\partial\phi}{\partial z} + \frac{\partial\phi_W}{\partial z}\right)^{n+1^\star}\end{aligned} \tag{30}$$

and Eq. (24) is changed to

$$\frac{\phi^{n+1}-\phi^n}{\Delta t} = \frac{1}{2}\left(-\frac{\partial\phi_W}{\partial t}+\frac{1}{2}\nabla\phi^2-gz\right)^n + \frac{1}{2}\left(-\frac{\partial\phi_W}{\partial t}+\frac{1}{2}\nabla\phi^2-gz\right)^{n+1}. \tag{31}$$

This variant is used throughout the paper. Carrying out this integration for the node at the intersection of the hull and the free surface does not necessarily lead to the node moving tangentially to the hull surface. Therefore, the position of this node is always corrected by shifting it normally to the hull surface. In the first time step an initial solution $\phi_0 = 0$, $z_0 = \zeta_W(x, y, t_0) = \zeta_{WA}\sin(\omega t_0 + kx)$ is applied, corresponding to a free surface where only the incident waves are present. The time step size is adjusted every time step so that

$$\Delta t \leq c\frac{\Delta s}{||\nabla\phi||}, \qquad 0 < c < 1 \tag{32}$$

is fulfilled at every node on the free surface. This guarantees that every node moves less than the local element size Δs.

Since the boundary conditions are not linearized with respect to the disturbance potential ϕ and evaluated at the actual instantaneous position of the free surface and the ship hull, large deformations of the free surface can be simulated. Because Eqs. (11) and (12) are substantial time derivatives, the nodes on the free surface are considered as fluid particles in the solution process described above. Since the boundary value problem for ϕ is solved in the Eulerian frame and the free surface is treated in a Lagrangian sense at the same time, the procedure described here is therefore called MEL-approach (Mixed Eulerian Lagrangian) and was used by Longuet-Higgins and Cokelet (1976) for the first time. The boundary element method used here follows the works of Sun (2007) and Greco (2001) and is described there in more detail.

To ensure the stability of the calculations in spite of the large deformations of the free surface, treatments of the numerical grid are necessary. The nodes of the free surface, which move differently due to the Lagrangian approach described above, have to be redistributed at each time step by regridding the free surface. The values of relevant properties at the new nodes are interpolated from the old nodes in this process using the same interpolation method as for the computation of the gradients described above.

Furthermore, a separation model is used to simulate flow detachment from curved hull surfaces. This model is based on the assumption, that ventilation occurs if the pressure on the hull close to the intersection is lower than atmospheric pressure. The model is very similar to the model developed by Sun (2007) and works as follows. If nodes on the hull surface next to the intersection node are detected where the pressure falls below atmospheric pressure, these nodes are then simply turned into free surface nodes thereby simulating ventilation. These nodes are then treated as free surface nodes in every way. In Fig. 4 this is the case for nodes A, B, C and D. Node A then becomes the new intersection node (see Fig. 5). Sun (2007) required the size of the low pressure area to be larger than a certain threshold size for flow separation to occur. A variation of the threshold size showed that although the location of the separation point fluctuates depending on the value of the threshold size, the computed forces are not significantly influenced. In the current model this threshold size corresponds to the size of an element. Therefore, the grid resolution has to be high enough in order to limit the grid dependence of separation. In the example shown in Figs. 4 and 5 employing the described model leads to a thin jet separating from the hull surface. In such cases numerical instabilities may occur near the jet tip (nodes B, C and D in Fig. 5). Therefore, a treatment similar as proposed by Bao et al. (2017) is employed. Since on both sides of the separated jet the pressure is atmospheric the pressure gradient can be assumed to be negligible here. The Euler equations for the separated jet area may then be written as

$$\frac{\mathrm{D}\mathbf{u}}{\mathrm{D}t} = -\frac{\nabla p}{\rho} - g\mathbf{k} = -g\mathbf{k}, \tag{33}$$

i.e. the velocities $\mathbf{u} = \nabla\phi + \nabla\phi_W$ can be updated directly at nodes B, C and D for the example in Fig. 5. As both ϕ and $\partial\phi/\partial n$ can then be computed directly, there are no unknowns at these nodes. This could of course be done for both sides of the jet. However, on some occasions small inaccuracies in the computed velocities led to both sides of the jet intersecting each other causing a breakdown of the simulation. For that reason it was decided to compute the values for $\partial\phi/\partial n$ on the other side of the jet from the BEM as for the other nodes on the free surface.

If separation is simulated this way, it may happen that reattachment occurs, see Fig. 6. Two different cases are considered. First, if the free surface intersects the hull surface, the node close to this intersection is then simply chosen as the new intersection node (node B in Fig. 6) and shifted normally to the hull surface so that it lies on the hull surface. Second, also a jet flow may again occur at the intersection, in which case node A is chosen to be the new intersection node if the angle between the free surface and the hull is beyond a certain threshold value, thereby gradually simulating the reattachment. This threshold value is chosen as high as possible, so that only problems regarding numerical stability due to poorly resolved jet flow are avoided. The reoccurring jet flow is detected from the computed velocities at the intersection node and the free surface node next to it. Both treatments can be

considered a rather simple modelling of what is actually happening. However, they are considered to capture the flow accurately enough so that the computations can be continued after the occurrence of reattachment.

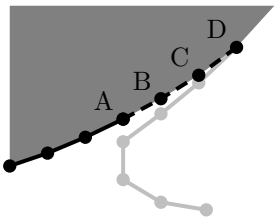

Figure 4: Negative pressure is detected at hull nodes A, B, C, D.

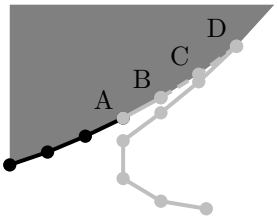

Figure 5: Hull nodes A, B, C, D are turned into free surface nodes.

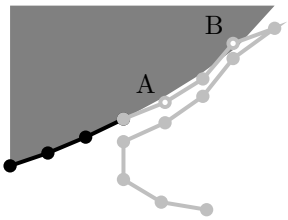

Figure 6: Reattachment may occur.

While it is possible to track separated or non-separated jets using the separation model described above, it is generally desirable to remove them from the fluid domain as their contribution to the forces acting on the hull surface is often negligible. Therefore attached as well as detached jets (spray) are from time to time cut off and new nodes are linearly interpolated between the cut nodes. This treatment has also been used by Kihara (2004, 2006) and Sun (2007) and is described there in more detail.

To sum up, the grid treatments employed here include detachment and reattachment by redefining the intersection node and cutting off thin jets and spray, where new nodes are inserted based on a linear interpolation between the cut nodes and regridding using a local second-order interpolation. Additionally, thin jets may be tracked where cutting them off is not possible. These treatments are carried out in that order at the beginning of each time step. Before updating the free surface as described above, the boundary value problem is solved once more, so that a complete solution is available.

The simulation using the method can be described as follows: At the beginning of the simulation, the ship is outside the computational domain which is formed by the several transverse earth-fixed cross planes. The ship moves into the domain at its speed U having its equilibrium running condition prescribed in the form of an initial sinkage $\xi_{30} = \xi_3(t = 0)$ and an initial trim angle $\xi_{50} = \xi_5(t = 0)$. In the first cross planes no waves are considered in the boundary conditions. When the ship has entered the domain completely, the incoming waves are also accounted for in the cross planes which still are in front of the ship at this point. When the ship moves through these sections, the solution of the equations of motion starts. The equilibrium forces $\mathbf{F}_0$, which are then considered, are determined beforehand in a simulation in calm water. After a short initial phase the motions become periodic. During the simulation new cross planes are constantly added in front of the ship, while those behind the ship are discarded as they are not needed to compute the forces acting on the ship.

EXPERIMENTS

The developed method is used to compute the dynamic behaviour of a semi-displacement vessel, which was studied experimentally by Keuning (1988) and Blok and Beukelman (1984). The body plan of the model is shown in Fig. 7 and its main dimensions and most important properties used for the computations in this paper are listed in Table 1. Two cases are considered here corresponding to Froude numbers Fn = 0.57 and 1.14.

Table 1: Case data (Keuning, 1988; Blok and Beukelman, 1984).

Froude number Fn [-]	0.57	1.14
Length L [m]	2	
Breadth B [m]	0.25	
Displacement M [kg]	12.48	
Pitch gyradius r_{55} [m]	0.5	
Longitudinal COG LCG [m]	0.898	
Vertical COG VCG [m]	0.068	
Initial trim angle ξ_{50} [°]	−1.2	−1.62
Initial sinkage ξ_{30} [m]	−0.001	0.007

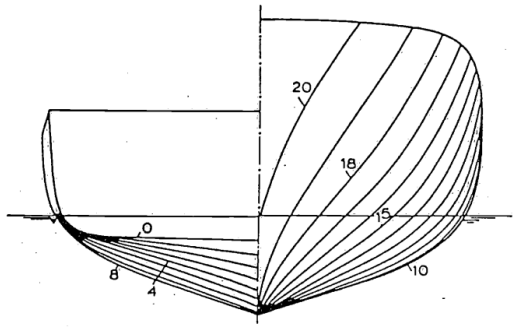

Figure 7: Keuning's model (Keuning, 1988).

Keuning's investigations were motivated by the experiments carried out earlier by Blok and Beukelman (1984). They studied the hull as part of the High-Speed Displacement Hull Form (HSDHF) series. In their experiments a systematic parametric study was carried out with respect to the influence on seakeeping performance. One of their findings was that in many cases the results obtained using strip theory correlated well with the experimental results also for high forward speed. Later Keuning (1988) used a model divided into seven segments in order to study in detail the distribution of the vertical force along the length of the model. He obtained the distribution of the vertical force at steady forward motion in calm water as well as the distribution of the unsteady vertical forces acting on the model performing an oscillatory forced heave motion at a certain frequency. In the latter case the results are presented in terms of added mass and damping coefficients.

RESULTS

Steady motion

First the case of steady forward motion in calm water is considered. The size of elements on the hull and the free surface near the hull is initially chosen as $\Delta s = 0.005\,\mathrm{m}$ based on a sufficient discretization of the hull surface and the expected free surface shape. The number of sections is similarly chosen as $N = 20$ so that variation of the sectional forces along the ship is captured with sufficient accuracy. The time step is chosen according to $c = 0.3$ in Eq. (32).

Fig. 8 and Fig. 9 show the free surface profiles obtained along the hull for Fn = 0.57 and Fn = 1.14, respectively. At Fn = 0.57 the simulation predicts moderate deformations of the free surface. Flow separation occurs in the bow area. At Fn = 1.14 the free surface deformations become much larger. The jet flow developing at the bow becomes more distinctive and extends further aft. The jet eventually separates from the hull and turns into a large bow wave propagating away from the hull.

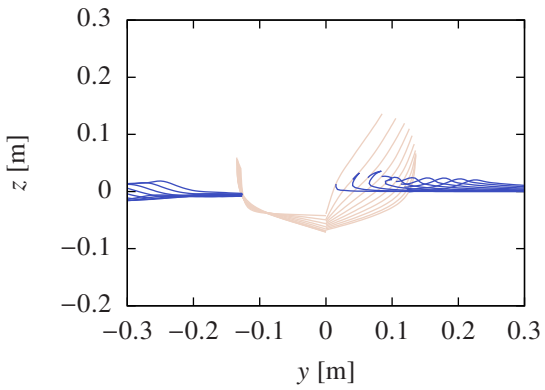

Figure 8: Computed free surface profiles at Fn = 0.57.

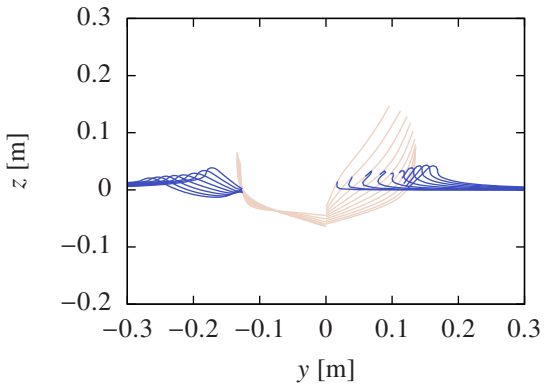

Figure 9: Computed free surface profiles at Fn = 1.14.

Following Keuning (1988), the vertical forces acting on the hull at Fn = 1.14 are studied in more detail. Fig. 10 shows the distribution of the computed vertical force. The total force has also been split up into a hydrostatic and a dynamic part. The hydrostatic part only considers the $-\rho g z$ term up to $z = 0$ during the pressure computation. The dynamic part is obtained by subtracting the hydrostatic part from the total force. As can been noticed in Fig. 10, dynamic pressures significantly contribute to the total force as may be expected at such high Froude number. In Fig. 11 the computed dynamic force is compared to measurements by Keuning (1988). While there is quite good agreement in the forward sections, differences between simulation and experiment can be seen near the transom stern. Due to the neglected three-dimensional effects (i.e. the fact that there is atmospheric pressure at the transom stern) the pressures and consequently the forces are significantly overpredicted in that area. In Fig. 12 the distribution

of the dynamic vertical force distribution for different vertical displacements $\eta_3 = \xi_3 - \xi_{30}$ is compared to the corresponding experimental results. Both computational and experimental results indicate larger changes with respect to η_3 at the stern than at the bow. As noted before significant deviations only occur at the transom stern.

Before continuing with the unsteady cases, the initially chosen values regarding spatial and temporal resolution are checked. Fig. 13 shows the variation of the sectional vertical forces with respect to element size. Only for the case of $\Delta s = 0.01$ there are notable differences in the bow area. In Fig. 14 the variation of the sectional vertical forces with respect to time step size are shown. No significant dependence can be observed. Based on these findings the initial choice of element size and number of sections are not adjusted. However, since in some of the cases with incoming waves instabilities occur with $c = 0.3$ when the motions at the free surface becomes more violent, the time step size is chosen according to $c = 0.2$. For simplicity these settings are used throughout the paper if not stated otherwise.

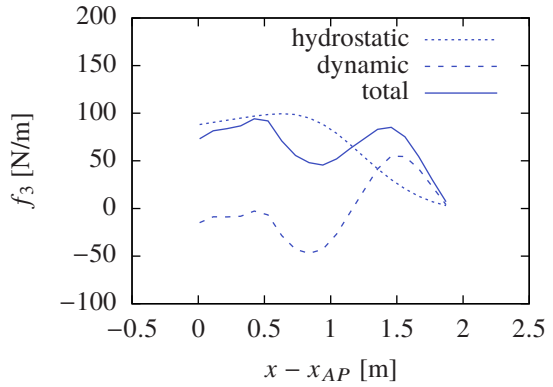

Figure 10: Computed vertical force distribution.

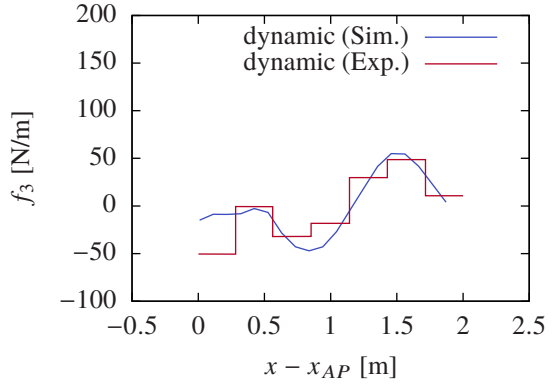

Figure 11: Computed dynamic vertical force distribution.

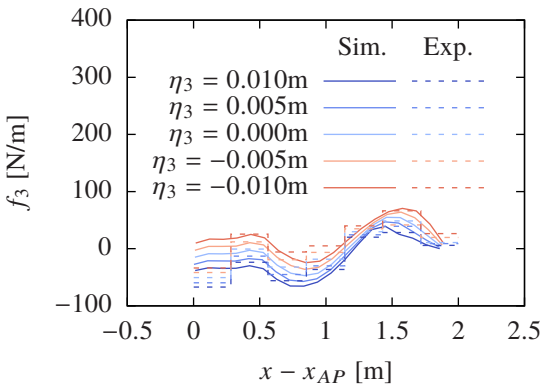

Figure 12: Computed dynamic vertical force distribution at different vertical displacements.

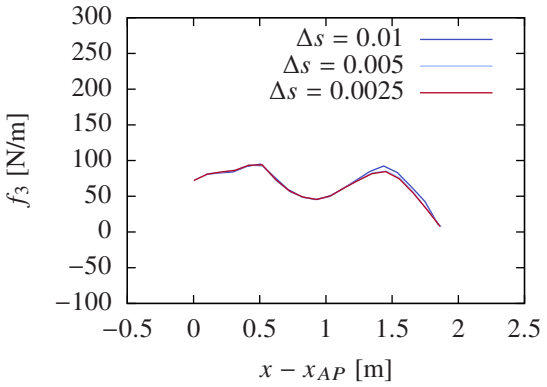

Figure 13: Computed vertical force distribution, element size varied.

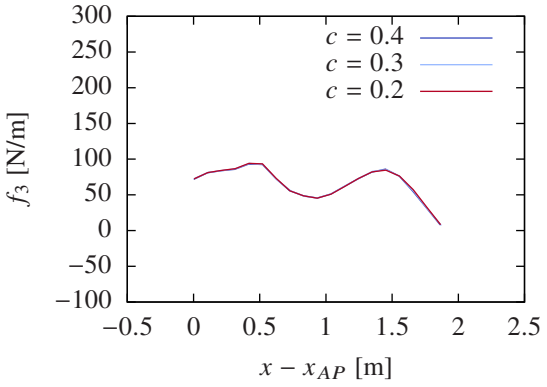

Figure 14: Computed vertical force distribution, time step size varied.

Forced motion

The cases of forced heave motion in calm water at forward speed are now considered. In these cases

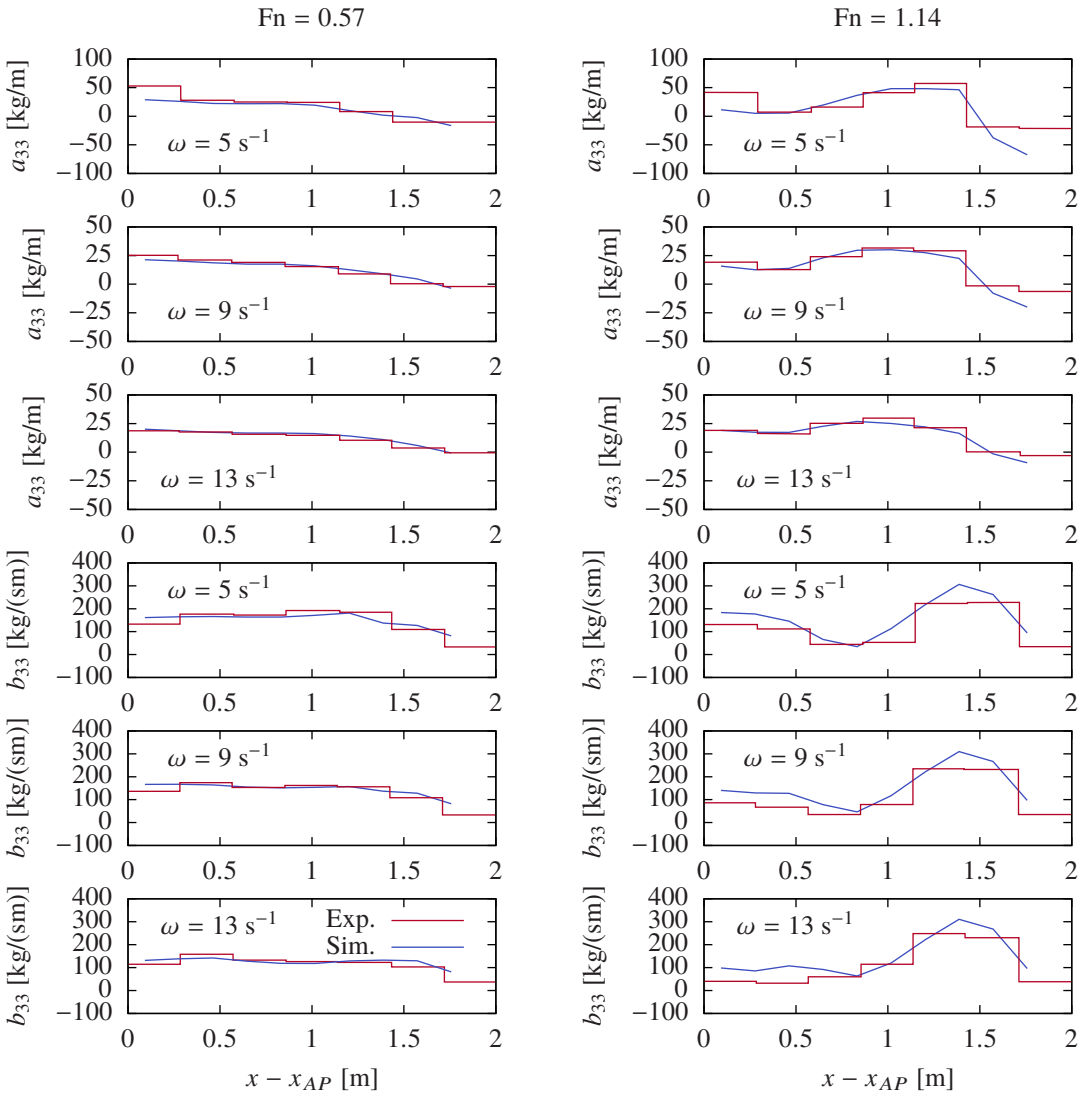

Figure 15: Computed sectional heave added mass and damping.

the ship moves into the fluid domain performing a prescribed harmonic heave motion at certain frequency and amplitude, i.e.

$$\eta_3 = \eta_{3A} \sin \omega t. \tag{34}$$

From the large amount of runs carried out during the experiments, the cases with heave amplitude $\eta_{3A} = 0.01$ m and frequencies $\omega = 5, 9$ and $13\,\mathrm{s}^{-1}$ are chosen here. The evaluation procedure is as follows: having obtained the time histories of the vertical sectional force at the several cross planes at earth-fixed locations x, the corresponding time histories at ship-fixed locations x'' can be computed using linear interpolation. Here, 10 ship-fixed locations have been chosen in the following analysis. Then for each section the vertical force f_3 is expanded into a Fourier series as

$$f_3 = a_0 + \sum_{n=1}^{\infty} (a_n \cos(n\omega t) + b_n \sin(n\omega t)). \tag{35}$$

Assuming

$$f_3 = -a_{33}\ddot{\eta}_3 - b_{33}\dot{\eta}_3 - c_{33}\eta_3 \tag{36}$$

the added mass and damping coefficients may be estimated from the first-order Fourier coefficients as

$$a_{33} = \frac{b_1 + c_{33}\eta_{3A}}{\omega^2 \eta_{3A}} \tag{37}$$

$$b_{33} = -\frac{a_1}{\omega \eta_{3A}}. \tag{38}$$

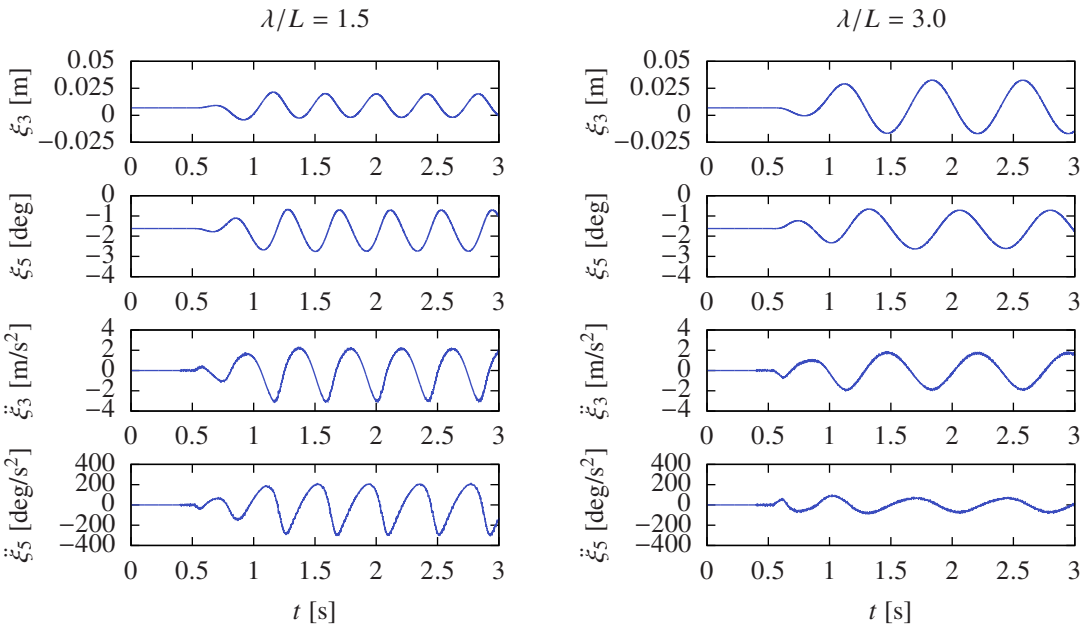

Figure 16: Computed heave and pitch motions at Fn = 1.14 for two different wave lengths.

Here $c_{33} = \rho g b$ is the sectional restoring coefficient, which is defined as in the experiments, b being the breadth at the waterline of the section under consideration. It is noted that due to the small trim angles the difference between the $x'y'z'$- and $x''y''z''$-coordinate system is neglected in this evaluation and $x_{AP} - x_G = x'_{AP} = x''_{AP} = -LCG$ is used.

Fig. 15 shows the results for the computed sectional added mass and damping coefficients for Fn = 0.57 and Fn = 1.14. The results for Fn = 0.57 are depicted on the left and the results for Fn = 1.14 are on the right. As mentioned before, three different frequencies are considered, $\omega = 5$, 9, and 13 s^{-1}.

The overall agreement between simulation and experiments is good. Differences appear especially at the bow and at the stern. Here neglected three-dimensional flow effects are expected to be more important. Especially the damping coefficients seem to be over-predicted at the transom stern. This effect seems to be much more pronounced for the higher Froude number. Other than the damping coefficients, the added mass coefficients seem to be under-predicted near the transom stern. However, this effect can be noticed only at the lowest frequency.

As mentioned by Sun and Faltinsen (2012), the interaction between steady and unsteady flow, which is accounted for in the present method, is more important at lower frequencies than at higher frequencies. Also as noted by Keuning (1988), better results can be expected at higher frequencies as the assumption of mainly two-dimensional flow is more appropriate in that case. The results obtained here seem to confirm this, as reasonable results are obtained for all frequencies, but agreement is generally better at higher frequencies.

The results may also be compared to those by Keuning (1988), who used two different linear strip methods to compute the sectional added mass and damping coefficients. However, in order not to overload the plots in Fig. 15, these results are not included here. The main difference between the two different strip methods was the way forward speed effects were handled. Keuning (1988) found both methods to have deficiencies at lower frequencies and at the higher Froude number Fn = 1.14. The present method performs better at lower frequencies and at higher forward speeds. That also shows that the interaction between steady and unsteady flow is important.

Free motion

The results presented so far have already been obtained in a very similar form by Sun and Faltinsen (2012). However, only Fn = 1.14 was considered. This approach is now extended to free motions in head waves, which, to the best knowledge of the authors, has not been done using a fully nonlinear potential flow method so far. The simulations considering incoming regular head waves are carried out as described above. As was done in the experiments by Blok and Beukelman (1984), the amplitude of the incoming waves is $\zeta_{WA} = 0.02$ m. Again two ship speeds corresponding to Fn = 0.57 and Fn = 1.14 are considered.

The results of the simulations are time series of the motions and forces acting on the ship. As an

example, Fig. 16 shows the results for the heave and pitch motions and accelerations for two different wave lengths, $\lambda/L = 1.5$ and $\lambda/L = 3.0$. Especially the time series of the accelerations show how the method works: for the first, say, 0.4 s of the simulation the ship is moving into the domain. The equations of motion are not solved during that time. As soon as the ship has entered the fluid domain completely the solution of the equations of motion starts. Small motions around the equilibrium running condition can then be observed. Their magnitude depends on the number of cross planes used and becomes smaller if the number is increased. No incoming waves are present in the first cross sections. As soon as the ship moves through cross planes in which the waves are taken into account in the boundary conditions, the motions become larger. Soon after the ship has completely entered the part of the domain where the waves are accounted for, the motions become periodic.

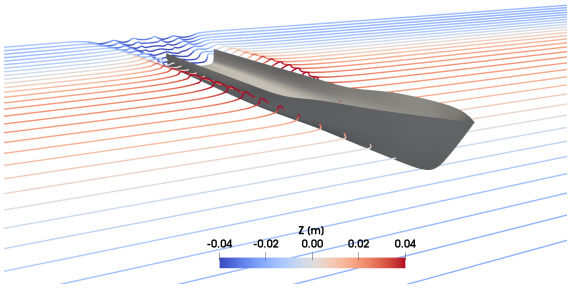

Figure 17: Snapshot of the simulation for Fn = 1.14 and $\lambda/L = 1.5$ at $t = 1.5$ s corresponding to the time instant where the pitch acceleration reaches its maximum.

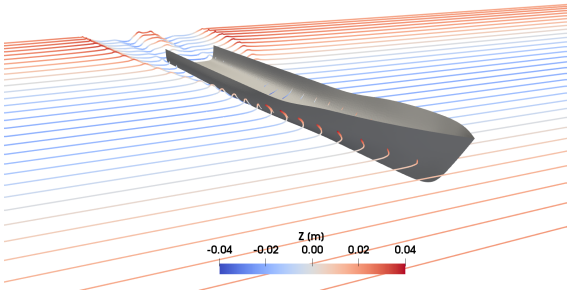

Figure 18: Snapshot of the simulation for Fn = 1.14 and $\lambda/L = 1.5$ at $t = 1.7$ s corresponding to the time instant where the pitch acceleration reaches its minimum.

Figs. 17 and 18 show screenshots from the simulation of the case Fn = 1.14 and $\lambda/L = 1.5$ at the time instants $t = 1.5$ s and $t = 1.7$ s, respectively. From the time series of the pitch acceleration depicted in Fig. 16 it can be seen that at these time instants the pitch acceleration reaches its maximum negative and positive values. As may be expected the maximum positive acceleration, which corresponds to a pitch moment forcing the bow to go down, is experienced on the wave crest. Similarly, the maximum negative acceleration is experienced when the bow hits into a wave trough. As can be seen in Fig. 18 a large amount of spray then develops in the fore ship. Also, the absolute value of the maximum negative acceleration is significantly larger than the absolute value of the maximum positive acceleration. This emphasizes the importance of nonlinearities in this case which can be captured using the present method. Nonlinearities also influence the accelerations in the case of $\lambda/L = 3.0$. However, their influence seems to be less obvious.

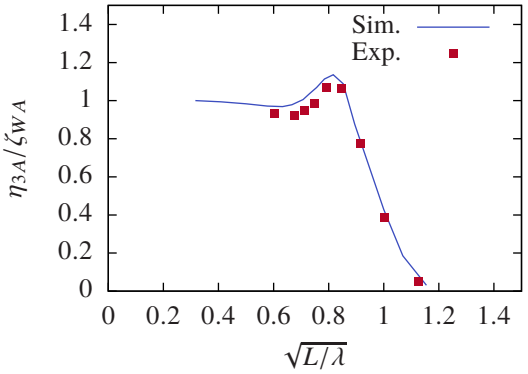

Figure 19: Computed heave amplitudes at Fn = 0.57.

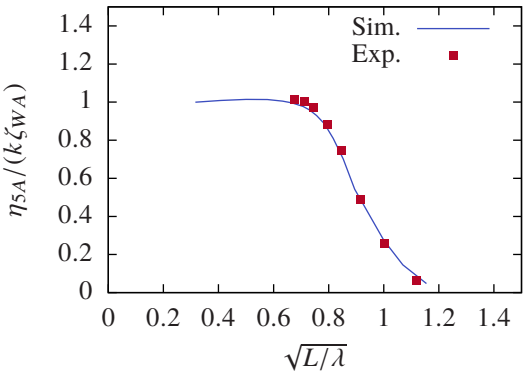

Figure 20: Computed pitch amplitudes at Fn = 0.57.

From the time series the heave and pitch amplitudes can be computed. The corresponding results are shown in Figs. 19 to 22. A very satisfactory overall agreement between numerical and experimental results can be seen. Only the results for the heave amplitudes at the lower Froude number Fn = 0.57 deviate slightly from the

experimental results. Since the deviations appear at larger wavelengths corresponding to lower encounter frequencies the reason could be the importance of accounting for the interaction of steady and unsteady flow. Although that is generally taken into account, due to the neglection of three dimensional effects, the steady flow can be expected to be better captured at higher Froude numbers than at lower Froude numbers, where transverse waves created by the ship may have a bigger influence. However, the results for added mass and damping coefficients seem to agree well also at lower frequencies, see Fig. 15. It may be interesting to investigate the coupling coefficients a_{35} and b_{35} as well. However, experimental results have only been presented for the heave motion by Keuning (1988). Sun (2007) investigated added mass and damping coefficients for heave and pitch for planing vessels using a 2D+t method and found deviations to be largest for A_{35} and B_{35}, particularly for lower frequencies. One could attempt to improve the agreement between experimental and numerical results by applying a correction to account for otherwise neglected three-dimensional effects.

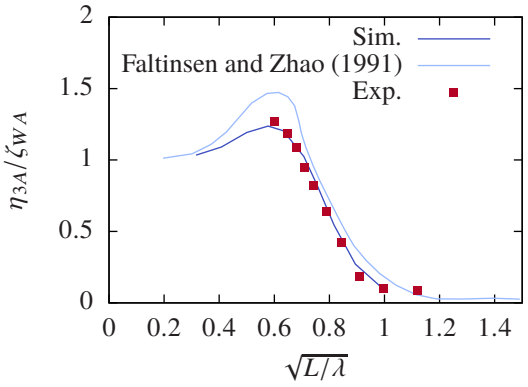

Figure 21: Computed heave amplitudes at Fn = 1.14.

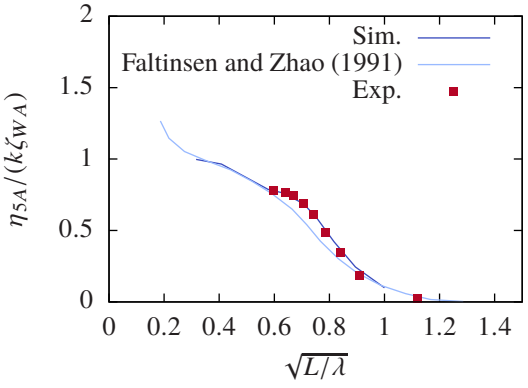

Figure 22: Computed pitch amplitudes at Fn = 1.14.

In Figs. 21 and 22 the results obtained using the 2D+t method by Faltinsen and Zhao (1991) are also shown. In their method, nonlinearities in the steady flow were accounted for, but the unsteady flow problem was linearized. This may be the reason why the current fully nonlinear method agrees better with the experiments near the resonance frequency. The current method also agrees generally better with the experimental results than the results of the two strip methods presented by Blok and Beukelman (1984), although they perform better than might be expected at such high Froude numbers based on their assumptions made about the flow. Additionally, simulations using these methods need much less computational time and are also more stable as the motion of the free surface does not need to be computed. Using the present method, stability issues were encountered in some simulations at higher encounter frequencies and near the resonance frequency. As mentioned before, these issues were solved by using $c = 0.2$ instead of $c = 0.3$.

CONCLUSIONS

A 2D+t method which is based on works by Sun (2007) and Sun and Faltinsen (2011) has been presented. This method replaces the three-dimensional flow problem around the ship by several two-dimensional time-dependent flow problems in earth-fixed transverse cross planes. The flow within each cross plane is treated as fully nonlinear potential flow satisfying nonlinear boundary conditions and solved using a BEM. Grid treatments like cutting off spray and jet flow developing in the bow area and a separation model are employed. Therefore, this method is able to account for many important features of the flow around semi-displacement hulls, such as the highly accelerated jet flow at the bow and separation of the flow from the round bilges and the dry transom stern. The method has been applied to cases of steady and unsteady motions of semi-displacement vessels in calm water and incident waves. While forced motions in calm water had already been considered earlier (Sun and Faltinsen, 2012), such a method has not been used before to compute free motions of semi-displacement vessels in incoming waves. In general, very satisfactory agreement between experimental and numerical results has been obtained. However, three-dimensional effects have been found to influence the results, particularly at lower frequencies. Corrections may be applied to improve the results in that respect. It is also suggested to extend the study of added mass and damping coefficients to the pitch motions, and the corresponding coupling coefficients, to find the reason for remaining differences between experimental and numerical results. Additionally, not only heave and pitch motions may be considered. Furthermore, improvements of the currently-used separation model seem necessary.

REFERENCES

Bao, C. M., Wu, G. X. and Xu, G., "Simulation of freefall water entry of a finite wedge with flow detachment," Applied Ocean Research, Vol. 65, 2017, pp. 262-278.

Blok, J. J. and Beukelman, W., "The High-Speed Displacement Ship Systematic Series Hull Forms - Seakeeping Characteristics", SNAME Transactions, Vol. 92, 1984, pp. 125-150.

Faltinsen, O. M., Hydrodynamics of High-Speed Marine Vehicles, Cambridge University Press, 2005.

Faltinsen, O. M. and Zhao, R., "Flow Predictions Around High-Speed Ships in Waves," Mathematical Approaches in Hydrodynamics, Society for Industrial and Applied Mathematics, 1991, pp. 265-288.

Greco, M. , "A Two-dimensional Study of Green-Water Loading," Ph.D dissertation, Norwegian University of Science and Technology, Norway, 2001.

Keuning, J. A., "Distribution of added mass and damping along the length of a ship moving at high forward speed," Technical Report No.817-P, Delft University of Technology, Netherlands, 1988.

Kihara, H., "Numerical models of water impact," Proceedings of the 4th International Conference on High-Performance Marine Vehicles, 27-29 September, 2004, Rome, Italy.

Kihara, H., "A Computing Method for the Flow Analysis around a Prismatic Planing-Hull," Proceedings of the 5th International Conference on High-Performance Marine Vehicles, 8-10 November, 2006, Launceston, Australia.

Longuet-Higgins, M. S. and Cokelet, E. D., "The Deformation of Steep Surface Waves on Water I. A Numerical Method of Computation," Proceedings of the Royal Society London A, Vol. 350, 1976, pp. 1-26.

Lugni, C., Colagrossi, A., Landrini, M. and Faltinsen, O. M., "Experimental and Numerical Study of Semi-displacement Mono-hull and Catamaran in Calm Water and Incident Waves," Proceedings of the 25th Symposium on Naval Hydrodynamics, 8-13 August, 2004, St. John's, Canada.

Mola, A., Heltai, L. and DeSimone, A., "Wet and Dry Transom Stern Treatment for Unsteady and Nonlinear Potential Flow Model for Naval Hydrodynamics Simulations," Journal of Ship Research, Vol. 61, No. 1, 2017, pp. 1–14.

Nakos, D., Kring, D. C. and Sclavounos, P. D., "Rankine panel methods for transient free-surface flows," Proceedings of the 6th International Conference on Numerical Ship Hydrodynamics, 2-5 August, 1993, Iowa City, Iowa, USA.

Ommani, B., "Potential-Flow Predictions of a Semi-Displacement Vessel Including Applications to Calm-Water Broaching," Ph.D dissertation, Norwegian University of Science and Technology, Norway, 2013.

Salvesen, N., Tuck, E. O. and Faltinsen, O. M., "Ship Motions and Sea Loads," SNAME Transactions, Vol. 78, 1970, pp. 250-278.

Sichermannm, W., "Zur Simulation und Vorhersage extremer Schiffsbewegungen im natürlichen Seegang", Ph.D dissertation, Hamburg University of Technology, Germany, 2008.

Söding, H., "How to Integrate Free Motions of Solids in Fluids," Proceedings of the 4th Numerical Towing Tank Symposium (NuTTS 2001), 23-25 September, 2001, Hamburg, Germany.

Sun, H., "A Boundary Element Method Applied to Strongly Nonlinear Wave-Body Interaction Problems," Ph.D dissertation, Norwegian University of Science and Technology, Norway, 2007.

Sun, H. and Faltinsen, O. M., "Dynamic Motions of Planing Vessels in Head Seas," Journal of Marine Science and Technology, Vol. 16, 2011, pp. 168-180.

Sun, H. and Faltinsen, O. M., "Hydrodynamic forces on a semi-displacement ship at high speed," Applied Ocean Research, Vol. 34, 2012, pp. 68–77.

Wang, Q. X., "Unstructured MEL modelling of nonlinear unsteady ship waves," Journal of Computational Physics, Vol. 210, No. 1, 2005, pp. 368-385.

Wu, G. X. and Eatock Taylor, R. "Transient Motion of a Floating Body in Steep Water Waves," Proceedings of the 11th International Workshop on Water Waves and Floating Bodies, 17-20 March, 1996, Hamburg, Germany.

Zlatev, Z. Z., Milanov, E., Chotukova, V., Sakamoto, N., and Stern, F., "Combined Model-Scale EFD-CFD Investigation of the Maneuvering Characteristics of a High Speed Catamaran," Proceedings of the 10th International Conference on Fast Sea Transportation, 5–9 October, 2009, Athens, Greece.

DISCUSSION

Hui Sun, DNV GL Maritime Advisory, Section of Ship Hydrodynamics and Stability

The authors performed very nice work in this paper, which is about a numerical method to simulate the high-speed vessels in waves. It is greatly appreciated that the authors make proper references to my thesis and other publications.

The presented results agree quite well with the published numerical results and experimental results. The new contributions are mainly the simulated heave and pitch motions in head sea waves. This is potentially difficult in the numerical simulations, since the careful treatments of the separated flows from the round bilge and high accuracy in the predicted pressures and forces are required. The authors seem to accomplish this in a satisfactory way. One question related to the numerical scheme is the selection of the number of cross-planes. It says 10 sections in the paper. Did the authors perform a sensitivity study with respect to the number of the sections? E.g. will the results be similar if more cross-sections are selected?

The mostly concerned issue for the applied 2D+t method is the 3D effects neglected near the transom stern and in the bow. This can be an important reason for discrepancies between the numerical results and the experiments. How did you find the sectional force at AP (stern) and FP (bow). In Figure 15, there seem to be no value at AP and FP. The dynamic forces near AP and FP can be small, by since the position is far from CG, their contributions towards the pitch moment can still be prominent.

AUTHOR'S REPLY

Thank you very much for your comments and questions, each of which is addressed below.

Regarding the first question, generally 20 sections have been used for the computations. This number is considered to sufficiently capture the distribution of the vertical sectional forces considering the results shown in Fig. 10. When interpolating sectional added mass and damping coefficients at ship-fixed cross sections from the earth-fixed cross planes used in the computations, 10 sections have been used based on a similar reasoning. A variation of the number of ship-fixed sections interpolated from the earth-fixed cross planes is shown in Fig. 23.

With regards to the second question, the sectional force at the bow is assumed to be zero and the sectional force at the transom stern is linearly extrapolated from the two aftmost sections. This is also shown in Fig. 23. Therefore, no corrections have been made for three-dimensional effects, which certainly influence the forces at the stern and the bow, as pointed out in your question. However, this is believed to be less of an issue for semi-displacement hulls than for planing hulls.

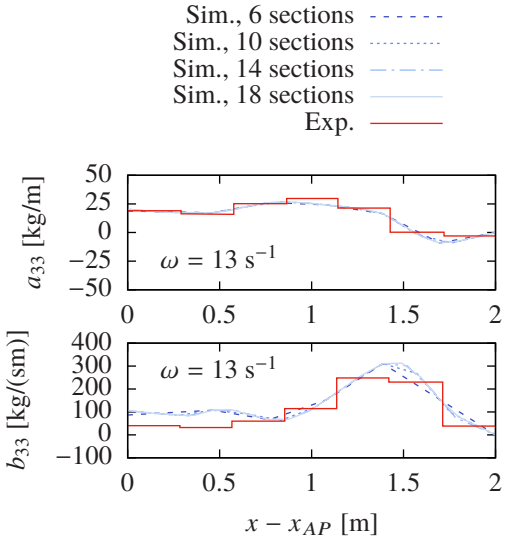

Figure 23: Computed sectional heave added mass and damping for different numbers of sections, Fn = 1.14.

DISCUSSION

Alessandro Iafrati, National Research Council, Institute of Marine Engineering (CNR-INM)

I thank the authors for such interesting work. The paper provides a significant advance on the development of an efficient method to study the dynamics of slender ships and high speed craft. There are only a few points I would ask the authors to explain more in detail.

1) The unsteady contribution to the pressure could be accurately computed by using the same BEM approach as done, for instance, in Battistin and Iafrati (2003). The BEM approach does not require to rebuild the matrix coefficients but only the known terms. Furthermore, it avoids the computation of the advective term in Eq. (28). Is there any specific reason why the BEM approach has not been used?

2) Page 5, right column: it is said that the coefficient matrix does not have to be recomputed during the iteration. I believe this is true for the subiterations at the same time step only, whereas the coefficient matrix needs to be updated from one time step to the next. Can authors better explain this point?

3) Page 6, just after Eq. (31): it is said that the hull-free surface intersection is not necessarily on the hull surface but it has to be shifted normally to the surface. However, this might affect the flow separation. Can authors better explain this point?

4) Page 6, left column, last paragraph: here, a separation model based on negative pressure is

used. There is experimental evidence that, in some circumstances, negative pressures may occur without flow separation (see Iafrati and Grizzi, 2019). The criteria might be too strong.

5) Generally, 2D+t models have troubles wherever there is a variation in the longitudinal direction. Examples are: bow/free-surface intersection, flow separation point, transom. This is clearly shown in Battistin and Iafrati (2003). Do authors use any correction at the bow to account for the pile up of the water? More important, can authors discuss how they account for the ventilation at the transom? The 2D+t approach generally predict a finite pressure at the transom, whereas a full 3D solution would predict a zero pressure with the ventilation effects propagating somewhat forward. This point is particularly important as it affect the ship dynamics.

REFERENCES

Battistin, D. and Iafrati, A., "A numerical model for hydrodynamics of planing surfaces," Proceedings of the 7th International Conference on Fast Sea Transportation, 7–10 October, 2003, Ischia, Italy.

Iafrati, A. and Grizzi, S., "Cavitation and ventilation modalities during ditching," Physics of Fluids, Vol. 31, 052101, 2019, pp. 1-14.

AUTHOR'S REPLY

Thank you very much for your comments and questions, each of which is addressed below.

1) Computing $\partial\phi/\partial t$ by solving an additional boundary value problem is generally considered to be both accurate and efficient. The reason for not using this approach is, that the body boundary condition, which has to be fulfilled, poses several difficulties. These involve evaluating second derivatives of the velocity potential and dealing with singularities at corners. That is why using this approach was postponed to a later stage.

2) That is fully correct. The coefficient matrix used in the BEM has to be updated when the shape of the free surface is updated according to Eq. (29) and (30). When the new value of the velocity potential at the free surface is determined iteratively according to Eq. (31), the coefficient matrix is not updated since the shape of the boundary does not change.

3) The flow separation point tends to fluctuate slightly during the computations. However, this seems to have a negligible influence on the computed forces. The separation model employed here is very similar to the model presented by Sun (2007), who showed the model to be convergent with respect to time step size and element size. Similar convergence studies have been carried out here, considering an impacting cylinder studied experimentally by Greenhow and Lin (1983). The cylinder has a radius of $R = 0.055\,\mathrm{m}$ and a mass per length of $m = \rho\pi R^2/2$ and is dropped from a height of $h = 2\,\mathrm{m}$, measured from the cylinder center to the undisturbed free surface. The computations start at $t = 0.3019\,\mathrm{s}$, assuming an initial vertical downward velocity of $2.961\,\mathrm{m/s}$ and an initial immersion of $0.002\,\mathrm{m}$, i.e. the details of the very early phase of the impact are neglected. This certainly influences the results, but since these computations are carried out to check the separation model, these assumptions are considered sufficiently accurate. Wagner's method is used to provide an initial solution for the free surface. Some of the results are presented in Figs. 24 to 26. In Fig. 24 flow separation can be seen to occur. In Fig. 25 the development in time of the horizontal location of the free surface intersection y_S can be seen. Three different element sizes have been used. Since $c = 0.4$ is used in every computation, also the time step size changes accordingly. Vertical accelerations $\ddot{\eta}_3$ are shown in Fig. 26. Since no significant dependence on grid resolution can be noticed, the separation model is considered to give convergent results with respect to spatial and temporal discretization and grid treatments.

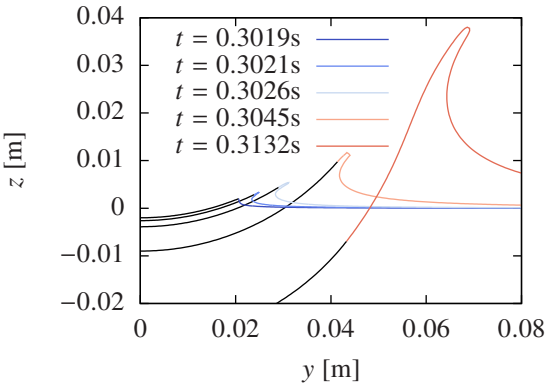

Figure 24: Impacting cylinder, free surface profiles.

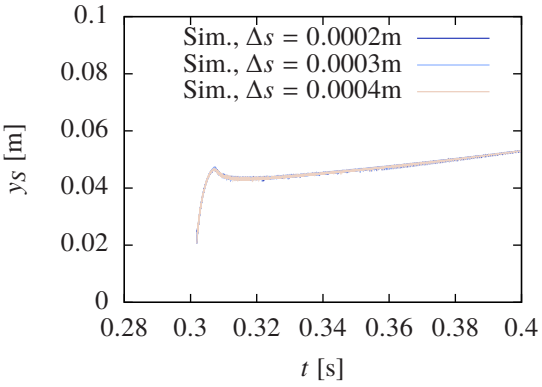

Figure 25: Impacting cylinder, horizontal location of the free surface intersection.

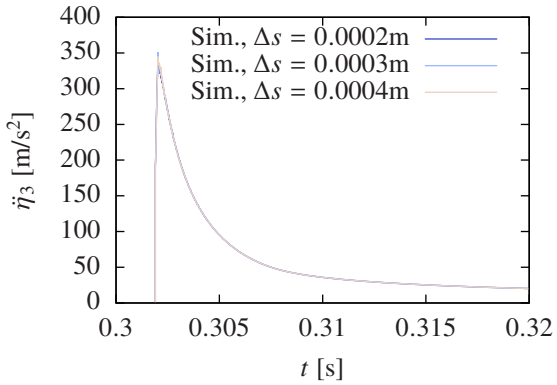

Figure 26: Impacting cylinder, vertical acceleration.

4) As stated in the conclusions, a further improvement of the separation model seems possible and also necessary to make it more stable and also more physical. We thank Dr. Iafrati for making us aware of recent results regarding ventilation and cavitation on impacting bodies. We will definitely consider the results presented by Iafrati and Grizzi (2019) in a further development.

5) The neglection of three-dimensionality of the flow is very important to keep in mind when using 2D+t models. No corrections with respect to three-dimensional effects have been considered so far. But we think that this is less of an issue for semi-displacement vessels than for planing vessels. The bow lines of semi-displacement vessels are usually very slender, so that no significant three-dimensionality may be expected at the bow. If there are no chines then there are also no issues regarding three-dimensionality of the flow, where the chines become wetted, as is the case when looking at planing vessels. However, there is no doubt that there is a three-dimensional effect at the transom stern, which is neglected. But since semi-displacement vessels usually have smaller forward speed and transom immersions than planing vessels, it is also considered less prominent.

REFERENCES

Greenhow, M. and Lin, W. M., "Nonlinear free surface effects: experiments and theory," Report No. 83-19, Department of Ocean Engineering, Massachusetts Institute of Technology, USA, 1983.